UCRL-ID-152002

A High-Wavenumber Viscosity for High-Resolution Numerical Methods

A.W. Cook, W.H. Cabot

February 19, 2003

U.S. Department of Energy

Lawrence
Livermore
National
Laboratory

DISCLAIMER

This work was performed under the auspices of the U. S. Department of Energy by the University of California, Lawrence Livermore National Laboratory under Contract No. W-7405-Eng-48.

Note

A high-wavenumber viscosity for high-resolution numerical methods

Andrew W. Cook and William H. Cabot

Lawrence Livermore National Laboratory, Livermore CA 94550

Key words: artificial viscosity, compact schemes, shock capturing

PACS: 47.11.+j

Numerical simulations of compressible flows are commonly based on the Euler equations when effects of viscosity are thought to be negligible. These equations admit singular solutions, even in cases where the initial and boundary conditions are smooth. So-called 'Euler solvers' rely on numerical dissipation, explicitly or implicitly present in the scheme, to regularize the problem, such that physical solutions are selected. In one dimension, the Euler equations for inviscid flow of an ideal gas are

$$\frac{\partial \rho}{\partial t} + \frac{\partial \rho u}{\partial x} = 0 \ , \tag{1}$$

$$\frac{\partial \rho u}{\partial t} + \frac{\partial}{\partial x}(\rho u u + p) = 0 \ , \tag{2}$$

$$\frac{\partial \rho E}{\partial t} + \frac{\partial}{\partial x}[(\rho E + p)u] = 0 \ , \tag{3}$$

$$p = (\gamma - 1)\rho e \ , \tag{4}$$

where ρ is density, u is velocity, p is pressure, $E = (e + uu/2)$ is total energy, e is internal energy and γ is the ratio of specific heats. Flows represented by discrete numerical 'solutions' to these equations are more consistent with a set of equations in which (2) and (3) are replaced by

$$\frac{\partial \rho u}{\partial t} + \frac{\partial}{\partial x}(\rho u u + p - \tau) = 0 \tag{5}$$

and

$$\frac{\partial \rho E}{\partial t} + \frac{\partial}{\partial x}[(\rho E + p - \tau)u] = 0 \ , \tag{6}$$

where τ is a dissipation mechanism, which produces entropy consistent with the Rankine-Hugoniot equations and the second law of thermodynamics. For schemes with implicit dissipation, various methods exist for estimating τ (Ramshaw, 1994). For the explicit-dissipation scheme to be introduced, we choose τ to be a stress term of the form

$$\tau = \mu \frac{\partial u}{\partial x} \ , \tag{7}$$

where μ is a grid-dependent artificial viscosity. Typically, as the grid spacing, Δx, goes to zero, $\mu \to 0$, but $\partial u / \partial x \to \infty$ at the discontinuities; therefore, τ remains finite at the discontinuities, regardless of grid refinement. Numerical simulations of discontinuous flows, like real-world flows, must generate finite entropy in the limit of vanishing viscosity; hence, numerical solutions are consistent with the Euler equations only in the sense that the space over which τ is nonzero decreases as $\Delta x \to 0$. The definition of a 'high resolution' numerical method is a scheme in which τ only damps wavenumbers close to the Nyquist wavenumber, $\pi / \Delta x$. For schemes with explicit artificial viscosity, this can be accomplished by making $\mu \propto \partial^r u / \partial x^r$, where r is a user-specified integer,

which gives the viscosity a high wavenumber (k^r) bias. This type of artificial selective damping has been successfully employed in acoustics computations by Tam et al. (1993), and by Barone and Lele (2002) who set $\tau \propto \partial^r u/\partial x^r$. In our formulation, we base μ, rather than τ on the r-derivative, in order to make (5) assume the form of the Navier-Stokes equation.

The effect of an added viscosity on the accuracy of a scheme can be quantified using the concepts of modified wavenumber and amplification factor. Consider a periodic isentropic flow, where (1), (2) and (3) can each be cast in the form

$$\frac{\partial \phi}{\partial t} + \theta \frac{\partial \phi}{\partial x} = 0 \ , \tag{8}$$

where θ is a wave speed and ϕ is a Riemann invariant (Landau and Lifshitz, 1959). For the purpose of analysis, θ will be taken as constant. The spatially-discrete analogue of (8) is

$$\frac{\partial \phi_j}{\partial t} + \theta D \cdot \phi_j = 0 \ , \tag{9}$$

where j is a grid index and $D\cdot$ denotes a discrete operator approximating $\partial/\partial x$. Fourier transforms ($\mathcal{F}$) of (8) and (9) can be written as

$$\frac{\partial \phi(k)}{\partial t} + \theta(ik/\Delta x)\phi(k) = 0 \ , \tag{10}$$

and

$$\frac{\partial \phi_k}{\partial t} + \theta(i\omega/\Delta x)\phi_k = 0 \ , \tag{11}$$

respectively, where $\phi(k) = \mathcal{F}\{\phi(x)\}$, $\phi_k = \mathcal{F}\{\phi_j\}$, k is a nondimensional wavenumber (ranging from 0 to π) and $\omega = \omega(k)$ is a nondimensional modified

wavenumber. The modified wavenumber for a spatial discretization of the form

$$\begin{aligned}&\beta\phi'_{j-2} + \alpha\phi'_{j-1} + \phi'_j + \alpha\phi'_{j+1} + \beta\phi'_{j+2} \\ &= c\frac{\phi_{j+3} - \phi_{j-3}}{6\Delta x} + b\frac{\phi_{j+2} - \phi_{j-2}}{4\Delta x} + a\frac{\phi_{j+1} - \phi_{j-1}}{2\Delta x}\ ,\end{aligned} \tag{12}$$

is obtained by taking the Fourier transform of (12) and applying the shifting theorem, $\mathcal{F}\{\phi_{j+m}\} = \exp(imk)\phi_k$. The result is (Vichnevetsky and Bowles, 1982; Lele, 1992)

$$\omega(k) = \frac{a\sin(k) + (b/2)\sin(2k) + (c/3)\sin(3k)}{1 + 2\alpha\cos(k) + 2\beta\cos(2k)}\ . \tag{13}$$

In this note, we will consider the following four centered differencing schemes: a 4th-order explicit (E4) scheme,

$$\alpha = 0\,,\ \beta = 0\,,\ a = \frac{4}{3}\,,\ b = -\frac{1}{3}\,,\ c = 0\,,$$

a 4th-order compact (C4) scheme,

$$\alpha = \frac{1}{4}\,,\ \beta = 0\,,\ a = \frac{3}{2}\,,\ b = 0\,,\ c = 0\,,$$

a 10th-order compact (C10) scheme,

$$\alpha = \frac{1}{2}\,,\ \beta = \frac{1}{20}\,,\ a = \frac{17}{12}\,,\ b = \frac{101}{150}\,,\ c = \frac{1}{100}\,,$$

and a spectral (S) Fourier transform scheme for which $\omega = k$.

The numerical amplification factor for a temporal integration method is defined as the solution (or error) after a complete time step $(n+1)$ divided by the solution (or error) at the previous time step (n), i.e., $A_N \equiv \phi_k^{n+1}/\phi_k^n$. Here we consider a five-step 4th-order Runge-Kutta (RK4) method derived

by Kennedy et al. (1999). For differential equations of the form $\dot{\phi} = f$, the scheme is

$$\begin{aligned} q^{\eta} &= \Delta t f^{\eta-1} + A^{\eta} q^{\eta-1} \\ & \qquad\qquad \eta = 1, ..., 5 \\ \phi^{\eta} &= \phi^{\eta-1} + B^{\eta} q^{\eta} \end{aligned} \tag{14}$$

where Δt is the time step, η is the RK4 subcycle, and A^{η} and B^{η} are:

$$A^1 = 0$$

$$A^2 = -6234157559845/12983515589748$$

$$A^3 = -6194124222391/4410992767914$$

$$A^4 = -31623096876824/15682348800105$$

$$A^5 = -12251185447671/11596622555746$$

$$B^1 = 494393426753/4806282396855$$

$$B^2 = 4047970641027/5463924506627$$

$$B^3 = 9795748752853/13190207949281$$

$$B^4 = 4009051133189/8539092990294$$

$$B^5 = 1348533437543/7166442652324\ .$$

This particular RK4 scheme was chosen for its broad stability properties for both convective and viscous terms. Applying (14) to (11) and combining all

the Runge-Kutta substeps leads to

$$A_N = \frac{\phi_k^{\eta=5}}{\phi_k^{\eta=0}} = \left[1 - \frac{\psi_\omega^2}{2} + \frac{\psi_\omega^4}{24}\right] - i\left[\psi_\omega - \frac{\psi_\omega^3}{6} + \frac{\psi_\omega^5}{200}\right] , \tag{15}$$

where $\psi_\omega \equiv \omega\Theta$ and $\Theta \equiv \theta\Delta t/\Delta x$ = CFL number. Numerical stability requires $|A_N| \leq 1$, and hence, the maximum stable CFL number depends on the maximum value of the modified wavenumber. Maximum stable CFL numbers for the E4-RK4, C4-RK4, C10-RK4 and S-RK4 schemes are 2.435, 1.929, 1.437 and 1.063, respectively.

The exact solution to (10) at $t = n\Delta t$ is $\phi^n(k) = \Phi\exp(-ikn\Theta)$. The amplification factor for the exact solution is

$$A_E \equiv \frac{\phi^{n+1}(k)}{\phi^n(k)} = \exp(-i\psi_k)$$

$$= \left[1 - \frac{\psi_k^2}{2} + \frac{\psi_k^4}{24} - \frac{\psi_k^6}{720} + \mathcal{O}(\psi_k^8)\right] - i\left[\psi_k - \frac{\psi_k^3}{6} + \frac{\psi_k^5}{120} - \mathcal{O}(\psi_k^7)\right] , \tag{16}$$

where $\psi_k \equiv k\Theta$. The total error (spatial plus temporal) for the centered-space Runge-Kutta schemes is $\mathcal{E}_N = A_N - A_E$. The real part of $\mathcal{E}_N$ is the diffusive error and the imaginary part is the dispersive error. The errors increase at higher wavenumbers and higher CFL numbers. Therefore, the optimum CFL number depends on the spectral content of the flow, and hence will vary depending on the problem.

To see how a wavenumber-weighted viscosity affects the overall error, add a term of the form $\nu k^r\phi(k)/\Delta x^2$ to the right-hand side of (10). The amplification factor for the exact solution with artificial viscosity is $A_V = \exp(\sigma k^r - ik\Theta)$, where ν is a kinematic viscosity parameter and $\sigma \equiv \nu\Delta t/\Delta x^2$. The error introduced by the spectral-like viscosity is

$$\begin{aligned}\mathcal{E}_V = A_V - A_E &= \exp(\sigma k^r - ik\Theta) - \exp(-ik\Theta) \\ &= \left[\sigma k^r + \mathcal{O}\left(k^{2r}\right)\right] - i\left[\sigma k^{r+1} + \mathcal{O}\left(k^{2r+1}\right)\right] \ .\end{aligned}$$

For small wavenumbers, k, we can choose r sufficiently large that $\mathcal{E}_V$ is less than $\mathcal{E}_N$; i.e., we can ensure that the error introduced by the artificial viscosity is less than the space-time discretization errors already present.

The particular form of explicit artificial viscosity employed in our simulations is

$$\mu = C_\mu \rho \Delta x^{r+1} \overline{\left|\frac{\partial^r u}{\partial x^r}\right|} \ , \tag{17}$$

where $\overline{|\ |}$ denotes a Gaussian filter applied to the absolute value. This is done in order to ensure that μ is smooth and positive. It is desirable to choose r as large as possible, in order to minimize the error caused by introducing τ into the equations. However, larger values of r require larger stencils to accurately represent the r-derivative. Compact (Padé) schemes provide a means whereby high derivatives can be computed with reasonably small stencils. For the current simulations we choose $r = 8$ and compute the 8th-derivative with the following compact scheme

$$\begin{aligned}29u_j^{VIII} + &\quad 14\left(u_{j+1}^{VIII} + u_{j-1}^{VIII}\right) \\ &+ (3/2)\left(u_{j+2}^{VIII} + u_{j-2}^{VIII}\right) \\ = [4200u_j &- 3360(u_{j+1} + u_{j-1}) \\ &+ 1680(u_{j+2} + u_{j-2}) \\ &- \ 480(u_{j+3} + u_{j-3}) \\ &+ \ \ 60(u_{j+4} + u_{j-4})]/\Delta x^8 \ ,\end{aligned}$$

where u_j^{VIII} approximates $\partial^8 u/\partial x^8$ at the jth grid point. The filter is then applied as

$$\overline{\left|u_j^{VIII}\right|} \equiv \frac{3565}{10368}\left|u_j^{VIII}\right| + \frac{3091}{12960}\left(\left|u_{j+1}^{VIII}\right| + \left|u_{j-1}^{VIII}\right|\right) + \frac{1997}{25920}\left(\left|u_{j+2}^{VIII}\right| + \left|u_{j-2}^{VIII}\right|\right) + \frac{149}{12960}\left(\left|u_{j+3}^{VIII}\right| + \left|u_{j-3}^{VIII}\right|\right) + \frac{107}{103680}\left(\left|u_{j+4}^{VIII}\right| + \left|u_{j-4}^{VIII}\right|\right) \ ,$$

which is very nearly equivalent to a Gaussian filter of width $4\Delta x$. For the calculations presented here, $C_\mu = 0.1$. Simulations in which the artificial terms are incorporated into the C10-RK4 scheme are denoted as C10V-RK4.

Our test problem is a breaking wave with initial conditions:

$$\begin{aligned} \rho/\rho_0 &= 1 + \epsilon \sin(2\pi x/\lambda) \\ p/p_0 &= (\rho/\rho_0)^\gamma \\ c_s/c_{s0} &= (\rho/\rho_0)^{(\gamma-1)/2} \\ u &= 2(c_{s0} - c_s)/(\gamma - 1) \ , \end{aligned}$$

where c_s is the sound speed, $\rho_0 = 10^{-3}$, $p_0 = 10^6$, $\gamma = 5/3$ and $\epsilon = 0.1$. The wavelength, λ, is set to $N\Delta x$, where N is the number of grid points per period. For this set of initial conditions, two of the three characteristics are initially constant, with the third satisfying a Burgers-like equation. The exact solution consists of the initial profiles being advected with velocity $u - c_s$, hence points on the profiles move from x to $\xi = x + (u - c_s)t$. A discontinuity begins to form when the solution attempts to become multivalued; this happens for a given x at

$$t = \frac{\lambda}{(\gamma+1)\pi\epsilon c_{s0}} \frac{[1 + \epsilon \sin(2\pi x/\lambda)]^{(3-\gamma)/2}}{\cos(2\pi x/\lambda)} \ ,$$

which has the minimum

$$\sin(2\pi x_b/\lambda) = -\frac{1}{(\gamma-1)\epsilon} + \left(\frac{1}{(\gamma-1)^2\epsilon^2} - \frac{3-\gamma}{\gamma-1}\right)^{1/2} \ .$$

For $\epsilon \ll 1$, $\sin(2\pi x_b/\lambda) \approx -(3-\gamma)\epsilon/2$ and $t_b = [\lambda/(\gamma+1)\pi\epsilon c_{s0}][1+O(\epsilon^3)]$, where t_b denotes the time when the wave first begins to break. The discontinuity therefore forms very near the point initially corresponding to $x = 0$ and grows to include more points on either side. The peaks of the initial sinusoidal profile at $x_p = \pm\lambda/4$ reach this point at a later time given by

$$t_p \approx \frac{(\gamma-1)(x_b - x_p)}{(\gamma+1)(c_{s,b} - c_{s,p})} \approx \lambda/2(\gamma+1)\epsilon c_{s0} \approx (\pi/2)t_b \ .$$

At this time, the discontinuity reaches its greatest amplitude, after which it slowly decreases (Landau and Lifshitz, 1959). The analytical solution to this breaking wave is only valid for $t \leq t_b$ because, unlike pure Burgers flow, the shock processes fluid; hence, the entropy ceases to be constant for $t > t_b$. The temporal evolution of the density field for the breaking wave is depicted in Fig. 1.

Convergence rates for the centered RK4 schemes at $t = 3t_b/4$, when the flow is still smooth, are plotted in Fig. 2. At high CFL numbers, time-stepping errors determine the rates of convergence; however, the actual errors are much lower for the higher-resolution spatial discretizations. For instance, errors for the C10-RK4 scheme are more than an order of magnitude lower than those of the E4-RK4 scheme, even though both methods are formally 4th-order accurate at CFL=1. At low CFL numbers, spatial discretization errors determine the rates of convergence; e.g., the C10-RK4 scheme exhibits 10th-order convergence at CFL=1/16. When artificial viscosity is added to this scheme, the convergence rate is limited by the r parameter, which in this case gives 8th-order convergence.

Next we compare the accuracy of the C10V-RK4 method against two standard

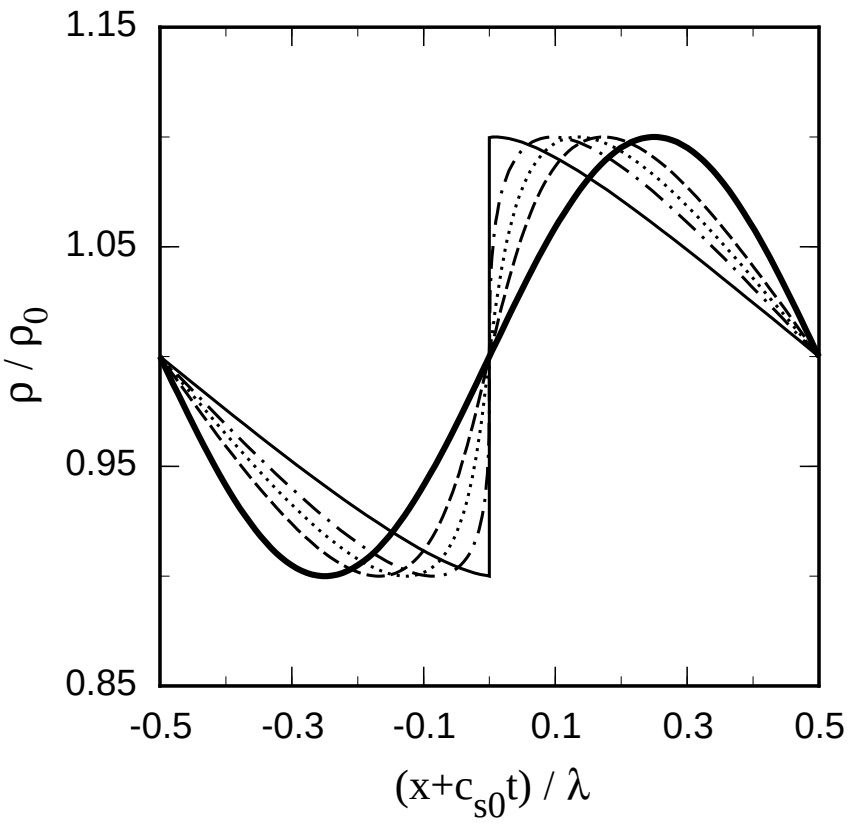

Fig. 1. Density solution in a frame moving with the mean wave velocity at $t = 0$ (heavy solid), $t_b/2$ (dashed), $3t_b/4$ (dotted), t_b (dot-dashed) and t_p (thin solid). At $t = t_b$ the wave has moved 1.19 periods in the fixed computational frame and at $t = t_p$ the wave has moved 1.87 periods.

shock-capturing methods, which have been published extensively in the literature, namely, Jiang and Shu's 5th-order Weighted Essentially Non-Oscillatory method with 3rd-order TVD Runge-Kutta time-stepping (WENO5-RK3) (Jiang and Shu, 1996), and Bell and Colella's 2nd-order Piecewise Linear MUSCL Direct Eulerian (PLMDE) method (Bell et al., 1989; Colella, 1990). Errors for the C10V-RK4, WENO5-RK3 and PLMDE methods are plotted versus time in Fig. 3 for CFL=1 and $N/\lambda = 128$. During the smooth phase, the error for the C10V-RK4 scheme is a couple orders of magnitude lower than the

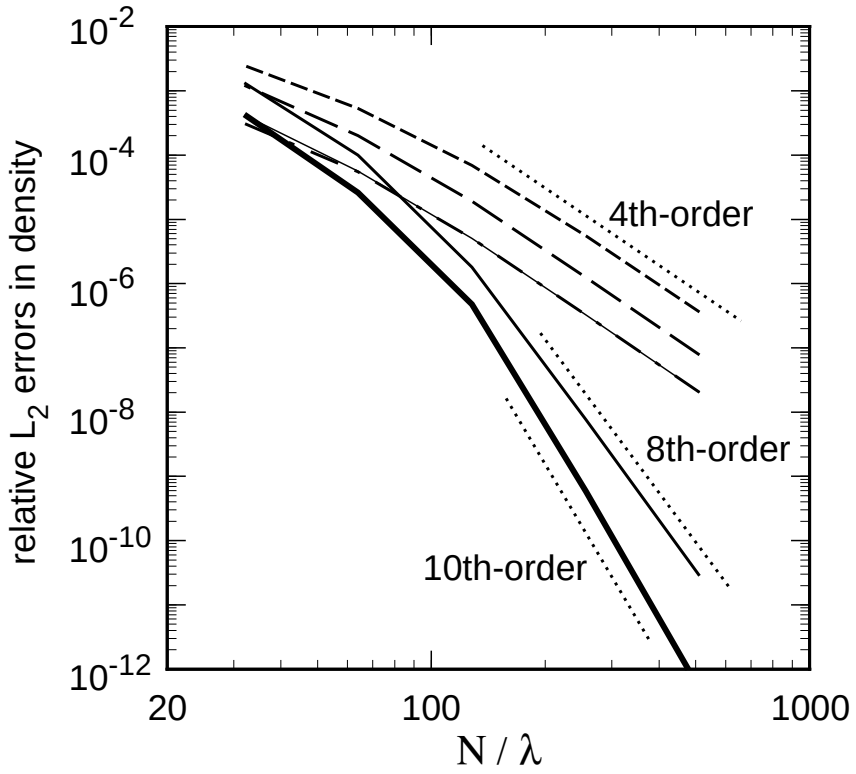

Fig. 2. Convergence rates for the centered RK4 schemes at $t = 3t_b/4$. Heavy solid line is C10-RK4 at CFL=1/16, medium solid line is C10V-RK4 at CFL=1/16, thin solid line is C10-RK4 at CFL=1, dot-dash line is S-RK4 at CFL=1 (this is nearly coincident with C10-RK4), long dashed line is C4-RK4 at CFL=1, short dashed line is E4-RK4 at CFL=1. Fiducial lines corresponding to 10th, 8th and 4th-order convergence are also plotted for reference.

WENO5-RK3 error, which, in turn, is about an order of magnitude lower than the PLMDE error. However, as the discontinuity forms, the errors for all three schemes become similar, and the rates of convergence all become first order. A scale-dependent measure of error is given in Fig. 4, which displays the density energy spectrum for the shock-capturing schemes at $t = 3t_b/4$ with $N/\lambda = 64$. The spectra provide a direct measure of the resolving power of each scheme. Two facts are evident from the plot; first, the C10-RK4 and C10V-

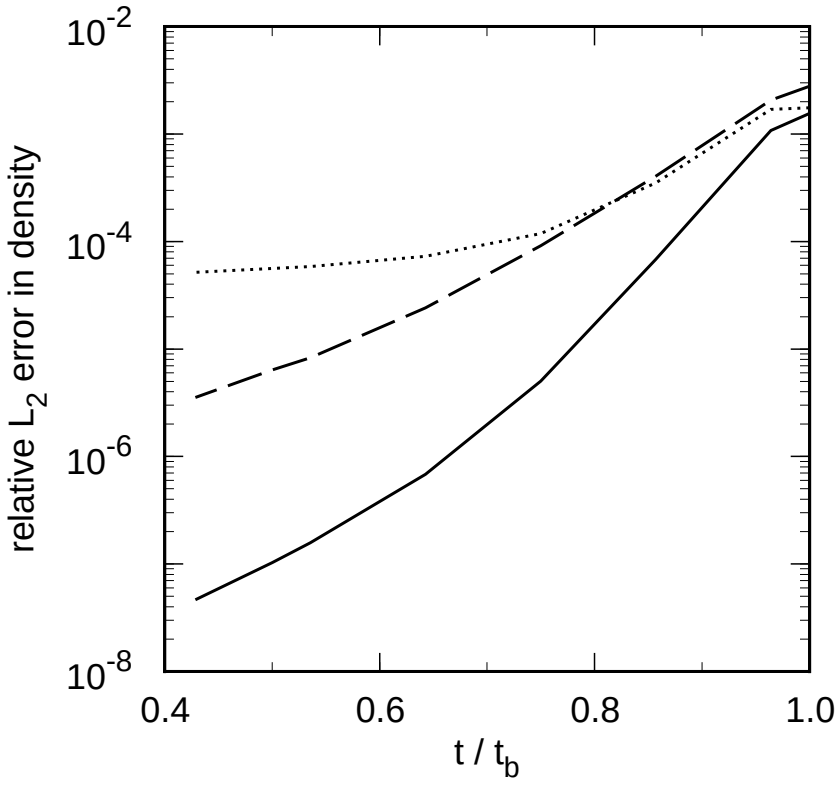

Fig. 3. L_2 errors for C10V-RK4 (solid), WENO5-RK3 (dashed) and PLMDE (dotted) at CFL=1 and $N/\lambda = 128$.

RK4 methods have nearly identical resolution properties, which means that the high-wavenumber viscosity has negligible impact on the solution in smooth regions; second, the C10 schemes give excellent representation for about half the wavenumbers, whereas the WENO5 and PLMDE schemes match less than a quarter of the wavenumbers. This is a consequence of the fact that the C10 schemes are purely centered, whereas the WENO5 and PLMDE methods are upwinded. The modified wavenumber for centered schemes is real (as is the true wavenumber), whereas the modified wavenumber for non-centered schemes is complex. For smooth flow, centered schemes have much greater resolving power than upwinded schemes.

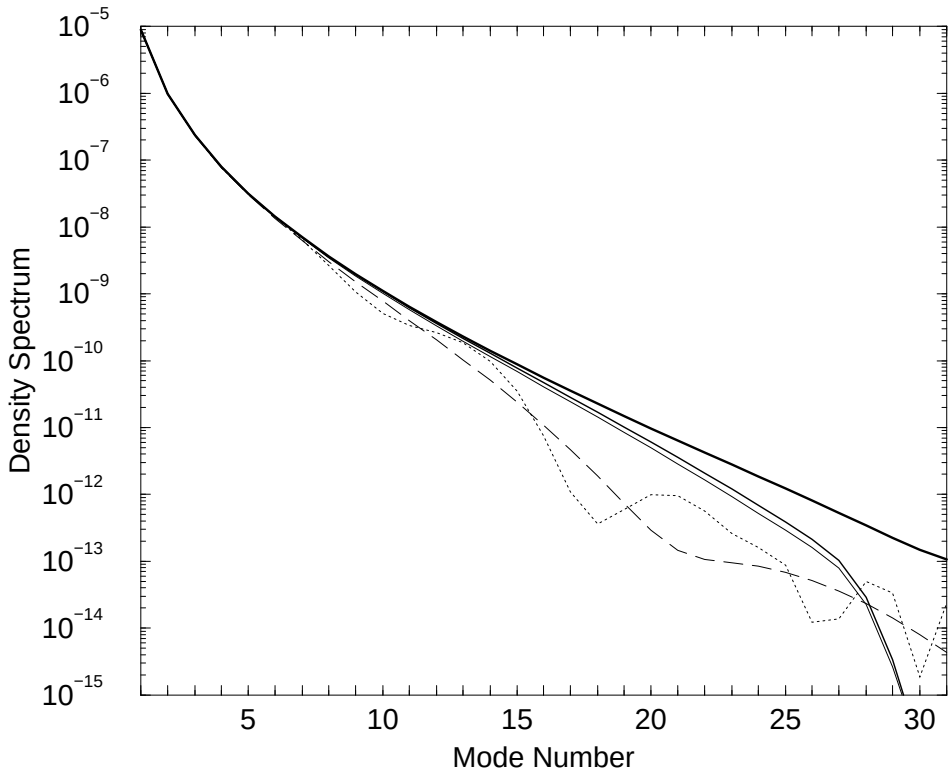

Fig. 4. Density spectrum at $t = 3t_b/4$ with $N/\lambda = 64$. Thick solid line is exact solution, medium solid line is C10-RK4, thin solid line is C10V-RK4, dashed line is WENO5-RK3 and dotted line is PLMDE. All numerical solutions computed at CFL=1.

In comparing the various numerical methods, a fundamental question is; what computational cost is required to compute the solution out to a certain time to within a specified accuracy? Table 1 displays times required for the various schemes to reach $t/t_b = 3/4$ (with CFL=1), at the resolution required to meet the indicated L_2 error. By this measure, the centered schemes are vastly more efficient than the upwinded methods, because they are able to satisfy the error tolerance with much fewer grid points. The particular numbers, of course, depend on the solution time and the specified tolerance; nevertheless, the centered schemes are clearly superior for smooth flow.

scheme	N/λ	time steps	CPU time (s)	L_2 error
E4-RK4	995	1004	1.467	2.03×10^{-8}
C4-RK4	715	722	0.777	2.03×10^{-8}
C10-RK4	512	516	0.583	2.03×10^{-8}
S-RK4	512	516	0.874	2.03×10^{-8}
C10V-RK4	512	516	1.40	2.03×10^{-8}
WENO5-RK3	2110	2157	76.0	2.03×10^{-8}
PLMDE	9900	9990	263	2.03×10^{-8}

Table 1

CPU times and resolutions required to reach $t/t_b = 3/4$, at CFL=1, to within the specified L_2 error.

The picture changes, however, when the flow becomes discontinuous. Fig. 5 displays the density solution for the C10V-RK4, WENO5-RK3 and PLMDE methods at $t = t_p$, the time at which the discontinuity reaches its greatest amplitude. For this time, the 'exact' solution is taken as the PLMDE result with $N/\lambda = 20,000$. For all three schemes, the shock is spread over about four grid points and spurious oscillations are negligible. Results for the C10-RK4 scheme (without artificial viscosity) exhibit strong Gibbs oscillations on both sides of the shock. The CPU times required for the C10V-RK4, WENO5-RK3 and PLMDE schemes to reach $t = t_p$ with $N/\lambda = 512$ and CFL=1, were 2.91, 9.76 and 1.424 seconds, respectively. The computational cost per time step is

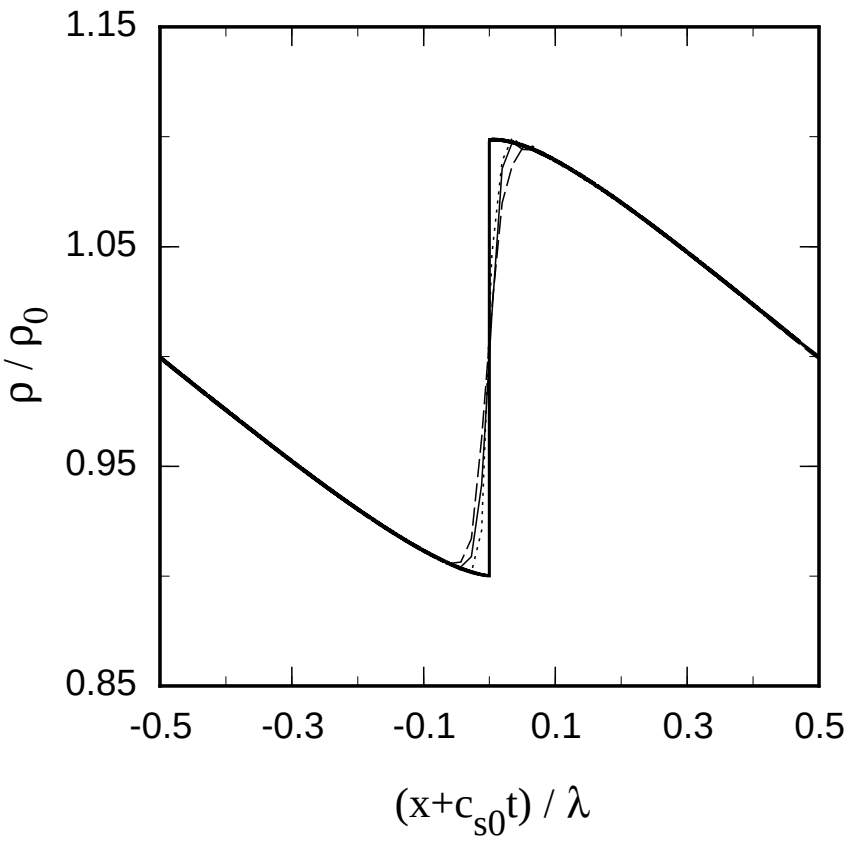

Fig. 5. Density computed with the PLMDE (dotted), WENO5-RK3 (dashed) and C10V-RK4 (thin solid) schemes at $t = t_p$ with $N/\lambda = 64$ using CFL=1. The thick solid line is the PLMDE solution with $N/\lambda = 20,000$.

least for the PLMDE scheme, so it is can clearly achieve a set level of accuracy in the post-break regime the most efficiently. The C10V-RK4 scheme is a close second in this regard, while the WENO5-RK3 is a more distant third due to its much greater expense.

In summary, we have proposed a high-wavenumber formulation for artificial viscosity as a means of stabilizing high-order methods and reducing oscillations near discontinuities. The spectral-like viscosity can be added to any numerical method, and is most conveniently implemented using compact sten-

cils to compute high derivatives. We have demonstrated the convergence rates for smooth flow to be proportional to the power of the derivative in the artificial viscosity; hence, the error introduced by the added dissipation can be made negligible in smooth regions by choosing a sufficiently high derivative. We combined the high-wavenumber viscosity with the most efficient of the centered schemes tested to produce an accurate and efficient shock-capturing method (C10V-RK4). The new C10V-RK4 scheme was evaluated against standard shock-capturing schemes (WENO5-RK3 and PLMDE). For the smooth flow phase, the C10V-RK4 scheme proved much more efficient than either the WENO5-RK3 scheme or the PLMDE method, with differences increasing for lower error tolerances. For the discontinuous phase of the flow, errors for the shock-capturing schemes were similar, and C10V-RK4 proved several times more efficient than WENO5-RK3 and about half as efficient as PLMDE.

Acknowledgements

We wish to thank Dr. W. J. Rider for providing the WENO code and Dr. J. A. Greenough for computing the WENO and PLMDE results. This work was performed under the auspices of the U.S. Department of Energy by the University of California Lawrence Livermore National Laboratory under contract No. W-7405-Eng-48.

References

Barone, M. F., Lele, S. K., 2002. A numerical technique for trailing edge acoustic scattering problems. AIAA paper 2002-0226, 40th AIAA Aerospace Sciences Meeting and Exhibit.

Bell, J. B., Colella, P., Trangenstein, J., 1989. Higher order Godunov methods

for general systems of hyperbolic conservation laws. J. Comput. Phys. 82, 362–397.

Colella, P., 1990. Multidimensional upwind methods for hyperbolic conservation laws. J. Comput. Phys. 87, 171–200.

Jiang, G.-S., Shu, C.-W., 1996. Efficient implementation of weighted ENO schemes. J. Comput. Phys. 126, 202–228.

Kennedy, C. A., Carpenter, M. H., Lewis, R. M., 1999. Low-storage, explicit Runge-Kutta schemes for the compressible navier-stokes equations. ICASE Report No. 99-22.

Landau, L. D., Lifshitz, E. M., 1959. Fluid Mechanics. Pergamon Press.

Lele, S. K., 1992. Compact finite difference schemes with spectral-like resolution. J. Comput. Phys. 103, 16–42.

Ramshaw, J. D., 1994. Numerical viscosities of difference schemes. Communications in Numerical Methods in Engineering 10, 927–931.

Tam, C. K. W., Webb, J. W., Dong, Z., 1993. A study of the short wave components in computational aeroacoustics. J. Comput. Acoustics 1, 1–30.

Vichnevetsky, R., Bowles, J. B., 1982. Fourier Analysis of Numerical Approximations of Hyperbolic Equations. SIAM, Philadelphia.